



Elastic and magnetic properties of Fe₃P up to core pressures: Phosphorus in the Earth's core

Xiaojing Lai^{a,b,*}, Feng Zhu^a, Yingxin Liu^{a,c}, Wenli Bi^{d,e}, Jiyong Zhao^d, E. Ercan Alp^d, Michael Y. Hu^d, Dongzhou Zhang^{a,f}, Sergey Tkachev^f, Murli H. Manghnani^a, Vitali B. Prakapenka^f, Bin Chen^{a,**}

^a Hawai'i Institute of Geophysics and Planetology, University of Hawai'i at Mānoa, Honolulu, HI, USA

^b Gemmological Institute, China University of Geosciences, Wuhan, Hubei, China

^c School of Gemmology, China University of Geosciences, Beijing, China

^d Advanced Photon Source, Argonne National Laboratory, Chicago, IL, USA

^e Department of Physics, University of Alabama at Birmingham, Birmingham, AL, USA

^f Consortium for Advanced Radiation Sources, University of Chicago, Chicago, IL, USA

ARTICLE INFO

Article history:

Received 13 May 2019

Received in revised form 8 November 2019

Accepted 16 November 2019

Available online xxxx

Editor: R. Dasgupta

Keywords:

sound velocities

density

magnetic transition

light elements

core composition

iron phosphide

ABSTRACT

Phosphorus (P) is considered a possible light element alloying with iron (Fe) in the Earth's core due to its siderophile nature and the ubiquity of P-bearing iron alloys in iron meteorites. The sequestration of P by liquid metals during the core formation possibly results in the relatively low concentration of P in the bulk silicate Earth. In this study, we performed single-crystal and powder X-ray diffraction, synchrotron Mössbauer spectroscopy and nuclear resonant inelastic X-ray scattering measurements in diamond anvil cells to investigate the elastic and magnetic properties of Fe₃P under high pressures. Our X-ray diffraction results suggest that there is no structural phase transition up to 111 GPa. However, a volume collapse was observed at 21.5 GPa in Fe₃P, ascribed to a magnetic transition as evidenced by synchrotron Mössbauer spectroscopy results. Fitting the volume-pressure data by the Birch-Murnaghan equation of state gives bulk modulus $K_{T0} = 162.4(7)$ GPa, its first pressure derivative $K'_{T0} = 4.0$ (fixed) and zero-pressure volume $V_0 = 370.38(6)$ Å³ for the magnetic phase and $K_{T0} = 220(7)$ GPa, $K'_{T0} = 4.0$ (fixed) and $V_0 = 357(1)$ Å³ for the non-magnetic phase. Sound velocities of Fe₃P were determined up to 152 GPa by nuclear resonant inelastic X-ray scattering, demonstrating that Fe₃P bears a low shear velocity and high Poisson's ratio at core pressures compared to Fe and Fe₃S. When forming a solid solution Fe₃(S,P) with Fe₃S at core pressures, Fe₃P may favorably influence the elastic properties of Fe₃(S,P) to match the seismic observations of the inner core.

© 2019 Elsevier B.V. All rights reserved.

1. Introduction

Earth's core is considered to consist of predominantly iron (Fe) alloyed with considerable amount of nickel (Ni) and one or more light elements, as inferred by numerous geophysical and geochemical studies (reviewed by Li and Fei, 2014). Light elements in the core such as silicon (Si), sulfur (S), oxygen (O), carbon (C) and hydrogen (H) are believed to be the culprit for the "density deficit" and sound velocity discrepancies between the high-pressure properties of Fe or Fe–Ni alloys based on mineral physics data and

seismic properties of the Earth's core from reference seismic models such as Preliminary Reference Earth Model (PREM) (Dziewonski and Anderson, 1981). The identity and concentration of principle light elements in the core are crucial for understanding the nature and dynamics of the core as well as the thermo-chemical evolution of Earth.

Compared to the likely major light alloying elements Si, S, O, C and H, phosphorus (P) may be a minor, but not trace, light element in the core. As a vital element in biological systems and metabolic pathways at the surface, P is present in only minute amount (0.09 wt.%) in the Earth's crust (Filippelli, 2008). The abundance of P in the mantle is also found to be well below the planetary volatility trend (McDonough, 2003), implying that significant amount of P may have entered the core during the core formation and that the core may be the largest reservoir of P. As a siderophile element,

* Corresponding author at: Hawai'i Institute of Geophysics and Planetology, University of Hawai'i at Mānoa, Honolulu, HI, USA.

** Corresponding author.

E-mail addresses: laixiaoj@hawaii.edu (X. Lai), binchen@hawaii.edu (B. Chen).

P could have preferentially partitioned into core-forming metallic liquids to form the proto core, with an estimated concentration of 0.2–0.5 wt.% in the core (McDonough, 2003; McDonough and Sun, 1995). Furthermore, Fe–P alloy such as schreibersite, $(\text{Fe,Ni})_3\text{P}$, is commonly found in iron meteorites, which are considered to be fragments of the cores of planets or planetesimals.

The occurrence of P in the solid core was suggested to be Fe_3P or $\text{Fe}_3(\text{S,P})$ (Gu et al., 2014; Stewart and Schmidt, 2007). At ambient conditions, Fe_3P adopts a tetragonal structure (space group $I\bar{4}$, $Z = 8$), isostructural with Fe_3S (Fei et al., 2000). The structural evolution of Fe_3P upon compression, however, remains controversial. A high-spin to low-spin transition at ~ 8 GPa was previously suggested from the change in compressibility by X-ray diffraction (XRD), followed by a phase transition from $I\bar{4}$ to unknown structure between 17 GPa and 30 GPa after laser annealing (Scott et al., 2007). However, more recent XRD and X-ray emission spectroscopy (XES) studies indicated a magnetic transition/spin transition at ~ 17 GPa, accompanied by a volume collapse, changes in the c/a ratio and diminishing of the satellite peak in the XES spectra (Gu et al., 2014; 2016). Gu et al. (2014) did not observe any phase transition at around 30 GPa but suggested a phase transition from $I\bar{4}$ to $P4/mnc$ space group at 64 GPa and 1650 K.

Iron-nickel sulfide and phosphide have been ubiquitously found in iron meteorites, typically coexisting with each other (Osadchii et al., 1981; Wasson, 2012). $(\text{Fe,Ni})_3(\text{S,P})$, the solid solution between schreibersite $(\text{Fe,Ni})_3\text{P}$ and its isostructural S-bearing iron alloy $(\text{Fe,Ni})_3\text{S}$ is a likely S- and P-bearing phase in the inner core, as $\text{Fe}_3(\text{S,P})$ solid solutions have been found in the liquidus phase relations of the Fe–S–P system from high-pressure and high-temperature experiments (Gu et al., 2016; Stewart and Schmidt, 2007). High-pressure studies on the magnetic and phase transitions, and elastic properties of Fe_3P can provide us with essential mineral physics data to evaluate the possibility of a P- and S-bearing core. To date, no elastic properties of Fe_3P have been reported after its magnetic transition and no sound velocity measurements have been performed for Fe_3P . In this study, single-crystal and powder XRD measurements at high pressures were conducted in the diamond anvil cells (DACs) to determine the densities, bulk moduli, as well as the plausible phase transitions of Fe_3P . Synchrotron Mössbauer Spectroscopy (SMS) and Nuclear Resonant Inelastic X-ray Scattering (NRIXS) measurements were conducted to investigate the magnetic transition and sound velocities of Fe_3P up to core pressures, respectively.

2. Materials and methods

Fe_3P samples were acquired from Alfa Aesar Company (99.5% purity) or synthesized using a large volume press. The synthesis of Fe_3P sample was carried out in the 2000-ton Walker-type multi-anvil apparatus at the University of Hawai'i at Mānoa (UHM). Starting materials were well mixed normal Fe (99.9+% purity, Aldrich Chemical Company) or ^{57}Fe (purity 98%+, #FLM-1812-0, Cambridge Isotope Laboratories Inc.) and P powders (98.9% purity, Alfa Aesar Company) with a stoichiometric 3:1 ratio. For each synthesis, the starting material (with normal Fe or ^{57}Fe) was loaded in a MgO sample capsule of COMPRES 10/5 cell assembly and cold compressed to 9 GPa. The sample was heated above its liquidus to 1873 K for 1 min, in order to melt and homogenize the sample. The temperature was then slowly decreased to 1423 K and kept at 1423 K for 27–31 h (Table S1). XRD measurements showed the commercial Fe_3P samples were pure large single crystals with lattice parameters $a = 9.110(1)$ Å, $c = 4.4630(4)$ Å, and $V = 370.43(5)$ Å³, and the synthetic samples were pure and polycrystalline Fe_3P with lattice parameters $a = 9.107(2)$ Å, $c = 4.463(2)$ Å, and $V = 370.13(23)$ Å³ (Fig. S1). The lattice parameters of the commercial and synthetic Fe_3P sam-

ples at ambient conditions agree with each other within uncertainties. Scanning Electron Microscope (SEM) and Energy Dispersive X-Ray Spectroscopy (EDS) measurements on those polished grains at the UHM also showed the samples belong to Fe_3P without any impurity. For synthetic $^{57}\text{Fe}_3\text{P}$ samples, trace amount of Fe was found in the sample charge. We screened the $^{57}\text{Fe}_3\text{P}$ samples to make sure the purity by XRD at the X-ray Atlas laboratory at the UHM before they were loaded to the DACs. The commercial Fe_3P was directly used for the single-crystal XRD experiments (run-1) and was ground for powder XRD (run-3). The synthetic Fe_3P and ^{57}Fe -rich Fe_3P were used in run-2 of the XRD experiment and all the NRIXS and SMS experiments, respectively.

2.1. Synchrotron-based single-crystal and powder XRD experiments

BX90-type and symmetric DACs with pairs of diamonds (250 μm or 100 μm culet sizes) were utilized in three runs of XRD experiments (Table S2). For the single-crystal XRD measurements, Boehler-Almax diamonds were used to maximize angular access to reciprocal space. Rhenium (Re) gaskets with initial thickness of ~ 270 μm were pre-indented to ~ 35 μm , where 150 μm and 60 μm -diameters holes were drilled as sample chambers for 250 μm and 100 μm culets, respectively. In run-1, a piece of single-crystal Fe_3P with a thickness of ~ 10 μm and a ruby sphere as a pressure calibrant were loaded in the sample chamber. In run-2, the synthetic Fe_3P sample with a thickness of ~ 10 μm was stacked on a piece of KCl pellet, which served as the pressure calibrant. In run-1 and run-2, neon was loaded into the sample chamber as the pressure transmitting medium using the gas loading system at GeoSoilEnviroCARS of the Advanced Photon Source (APS), Argonne National Laboratory (ANL). In run-3, ground Fe_3P were compressed into pellet and sandwiched by two pieces of 10- μm KCl pellets, which served as the pressure calibrant and pressure transmitting media. Due to its highly hygroscopic nature, KCl pellets were dried on a hot plate at 400 K for several hours before being loaded into the sample chamber. After the sample loading, the DAC with the sample chamber slightly exposed to the open air was placed in a vacuum oven at 383 K before being compressed to high pressure, in order to minimize the amount of the moisture introduced into the samples.

High-pressure single-crystal and powder XRD experiment (run-1 and run-2) were conducted at beamline 13-BMC, APS, ANL. The typical size of the focused monochromatic X-ray beam ($\lambda = 0.4340$ Å) was 16×11 μm^2 . A MAR165 charged coupled device (CCD) detector was used to collect the diffraction patterns. For the single-crystal XRD measurements (run-1), the X-ray accessible opening angle of the DAC was 59° . The rotation axis for the single-crystal diffraction experiment was placed horizontally, perpendicular to the incident X-ray beam. A series of 10° wide-angle exposures and 1° step exposures from -30° and 29° were collected at four different detector positions for each pressure point. The powder XRD experiment up to 111 GPa (run-3) were conducted at 13-IDD, APS, ANL. The typical size of the focused monochromatic X-ray beam ($\lambda = 0.3344$ Å) was 2.5×3.5 μm^2 . Double-sided laser heating system at beamline 13-IDD was used to anneal the sample to facilitate the potential phase transition and mitigate the deviatoric stress applied to the sample. The sample was gradually heated up to 2000 K with a heating duration of 6 to 9 mins and quenched to room temperature before the XRD patterns were collected. The temperature uncertainty is typically less than 100 K.

We utilized the ATREX software package for peak fitting and intensity corrections for the analysis of the single-crystal XRD data (Dera et al., 2013). The unit-cell parameters and orientation matrix were determined by the CELL_NOW software (Bruker AXS Inc.). Lattice parameters were refined by least-squares fitting in the

RSV software (Dera et al., 2013). The structure refinement of data at ambient conditions was performed using SHELXL (Sheldrick, 2008). Powder XRD patterns were integrated using Dioptas software (Prescher and Prakapenka, 2015). Synchrotron-based XRD patterns were fitted by PDindexer (Seto, 2010) and GSAS-II software (Toby and Von Dreele, 2013).

2.2. SMS and NRIXS measurements

A panoramic DAC containing diamonds with a 300 μm tip, 8° bevel angle, and 150 μm culets was used to generate pressure for the NRIXS and SMS measurements. Another symmetric DAC with 300 μm diamonds was also utilized for the SMS experiments. For the NRIXS and SMS measurements, a polycrystalline $^{57}\text{Fe}_3\text{P}$ sample with the thickness of ~ 30 μm was sandwiched between two thin KCl pellets and loaded into the sample chamber of a pre-indented beryllium gasket with a boron nitride epoxy insert. The boron nitride epoxy insert helps to reduce the axial pressure gradient and maintain sample thickness. A ruby sphere was placed next to the sample and served as a pressure calibrant (Mao et al., 1986). The Raman spectra of the diamond anvils were used as the pressure calibrant when the fluorescence of ruby became weak at >1 Mbar (Akahama and Kawamura, 2006). For the other SMS measurements, a ~ 15 μm -thick polycrystalline $^{57}\text{Fe}_3\text{P}$ sample was loaded into the sample chamber of a pre-indented Re gasket with the thickness of 35 μm . Neon as transmitting media and ruby spheres as pressure calibrant were also loaded into the sample chamber (Mao et al., 1986).

The NRIXS and SMS measurements were carried out at beamline 3-IDB, APS, ANL with the storage ring operating in the top-up mode with 24 bunches separated by 153 ns to obtain appreciable signal rates (Sturhahn, 2004). The X-ray energy was tuned around the nuclear resonance energy of ^{57}Fe at 14.4125 keV, and then NRIXS spectra were collected using three avalanche photodiode detectors (APDs) within the range from -70 to 130 meV with a step size of 0.25 meV and a collection time of 3–5 s per energy step. Multiple NRIXS spectra were collected until sufficient counts were obtained at each pressure. The SMS measurements were conducted using an APD placed downstream in the forward scattering direction. The PHOENIX program package was used to derive partial phonon density of state (PDOS) and extract Debye sound velocity (Sturhahn, 2000).

3. Results and discussion

3.1. Magnetic transition and compressibilities of Fe_3P up to Mbar pressures

Fe_3P adopts a close-packed crystal structure with a space group of $I4$ at ambient conditions (Fig. 1). Three runs of XRD measurements were carried out at high pressures. Run-1 was a single-crystal XRD experiment (Figs. S2A, S2B and S2C). Samples of run-2 and run-3 were polycrystalline and their XRD patterns could be integrated into 1-D spectra like powder XRD (Fig. S2D). In run-3, it was noted that a substantial impurity peak likely belongs to *hcp* Fe at high pressures (Fig. S2D). The majority of the peaks can be indexed as Fe_3P . The possible Fe peak does not overlap with the sample peaks and thus would not cause any bias to phase identification and equation of state. No structural phase transition was observed in this study, even after repeated laser annealing up to the highest pressure of 111 GPa. This is not consistent with the report by Gu et al. (2014), which suggested a phase transition in Fe_3P at 64 GPa and 1650 K after laser annealing. The cause of the inconsistency remains unclear, but the factors such as recrystallization of the sample after laser heating might cause some changes in XRD patterns that may not result from a phase transition.

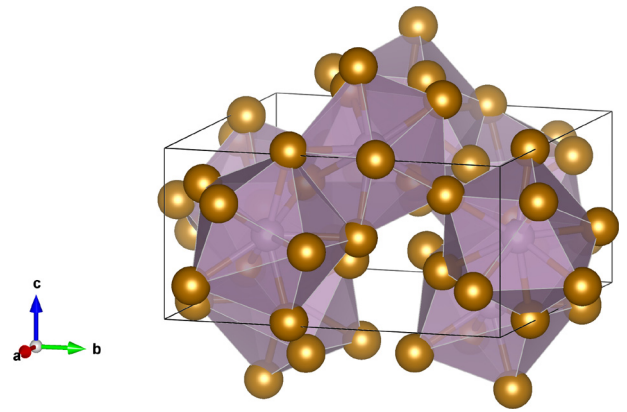


Fig. 1. Crystal structure of Fe_3P at ambient conditions refined by single-crystal XRD data in this study. Purple balls in polyhedra represent the P atoms and brown balls represent Fe atoms. Each P atom was surrounded by 9 Fe atoms to form nine-fold coordination polyhedron. (For interpretation of the colors in the figure(s), the reader is referred to the web version of this article.)

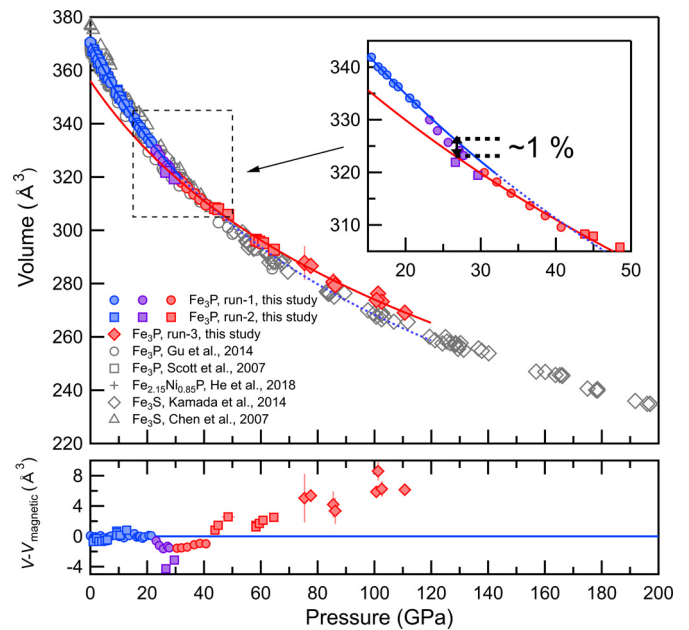


Fig. 2. Unit-cell volume of Fe_3P as a function of pressure at 300 K. Solid symbols represent the data in this study, and open symbols represent the data in other studies (Chen et al., 2007; Gu et al., 2014; He et al., 2018; Kamada et al., 2014; Scott et al., 2007). Symbols are blue for the magnetic phase of Fe_3P , red for the non-magnetic phase of Fe_3P , and purple for the phase during the transition. Data below 21.4 GPa and data above 30.5 GPa in this study were fitted by the second order BM-EoS (solid and dashed blue lines and red solid line). Inset shows the zoom-in range in which the transition occurred. Bottom figure shows the volume difference between the volume of Fe_3P and the volume calculated using the equation of state of the magnetic phase.

During compression, we observed a continuous volume collapse in Fe_3P starting from approximately 21.4 GPa by the XRD experiment (Fig. 2). The P - V data up to 21.4 GPa and at 300 K (Tables S3 & S4) can be well fitted by the 2nd-order Birch-Murnaghan Equation of State (B–M EoS). The volume difference between the actual volume and the calculated volume by the equation of state is almost zero up to 21.4 GPa (Fig. 2). It is noted that the single crystal XRD data are much less scattered than the powder XRD data, because there are significant more peaks with different *hkl*s permitting better constraining the lattice parameters. Above 21.4 GPa, the volume of Fe_3P is lower than the calculated volume and the volume difference became larger up to 30.5 GPa (Fig. 2). After 30.5 GPa, the volume difference became smaller and positive at

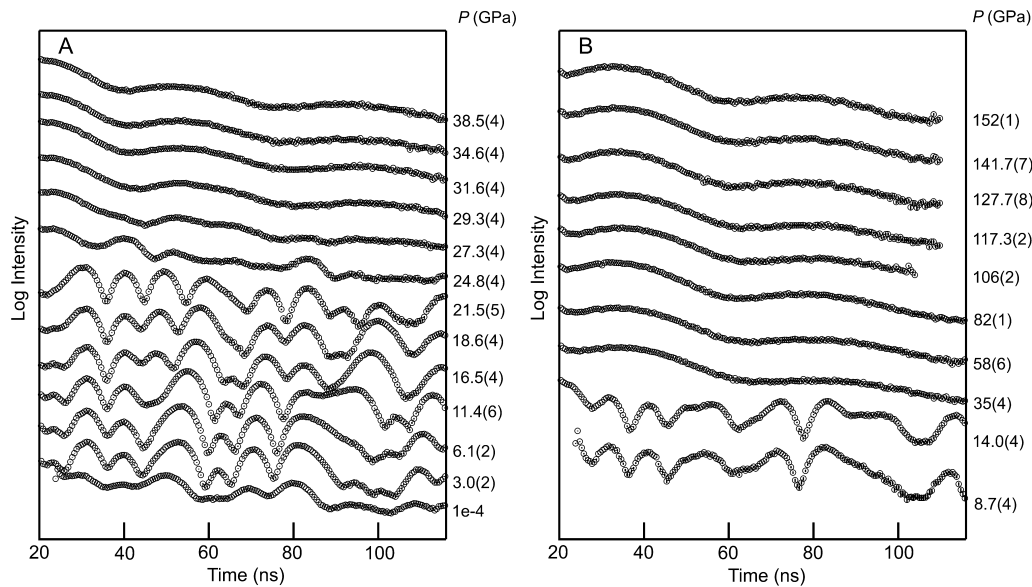


Fig. 3. Synchrotron Mössbauer spectra of Fe_3P at high pressures. (A) Synchrotron Mössbauer data collected in a symmetric DAC. (B) Synchrotron Mössbauer data collected in the panoramic DAC along with NRIXS data collection. Magnetic moment started to diminish between 21.5 GPa and 24.8 GPa. Magnetism completely disappeared at around 31.6 GPa.

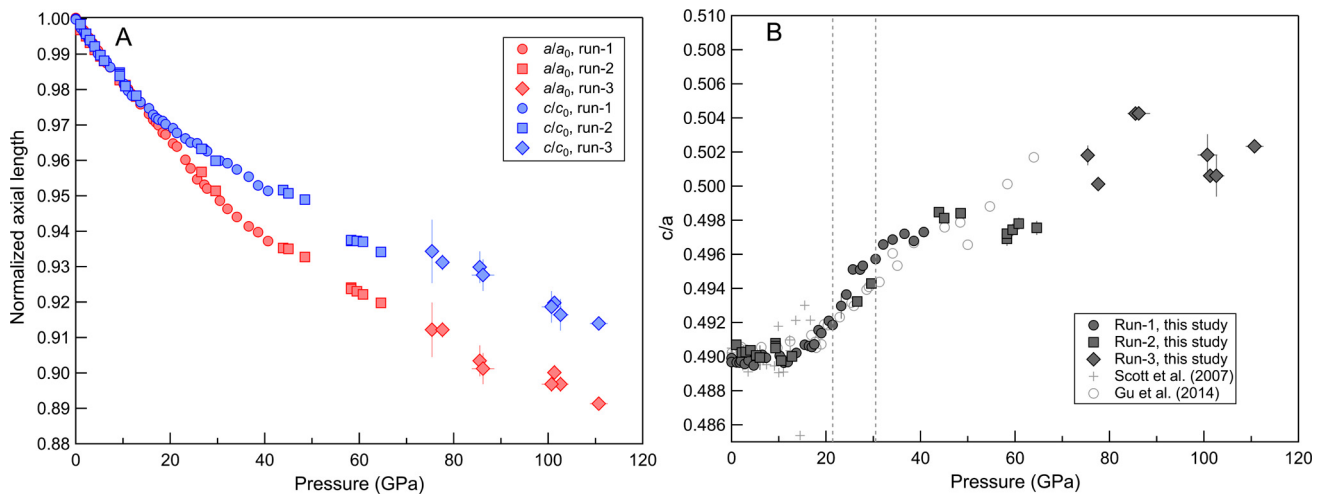


Fig. 4. (A) Normalized axial lengths and (B) c/a ratio as a function of pressure. Solid symbols represent data from this study. The open grey symbols represent data from other studies (Gu et al., 2014; Scott et al., 2007) for comparison. The dashed lines represent the starting and ending pressures of the magnetic transition indicated by our XRD experiments.

even higher pressure due to the stiffening of Fe_3P after the transition. The observed volume drop of $\sim 1\%$ is consistent with 1–2% drop reported by Gu et al. (2014) (Fig. 2, inset). It coincides with the pressure-induced magnetic transition starting at 18.3 GPa reported in previous XRD and XES studies (Gu et al., 2014; 2016). Our SMS results further confirmed the magnetic transition (Fig. 3). Below 21.5 GPa, the magnetic splitting is manifested as obvious fast oscillations in the SMS spectra (Sturhahn, 2000) (Fig. 3). Upon further compression to 29.3 GPa, the magnetic moment diminished substantially and completely disappeared at 31.6 GPa. The SMS technique is a sensitive local probe of very small transferred hyperfine fields. There are three different Fe sites in Fe_3P and each Fe site may undergo its own path of magnetic transition under compression. As a result, the disappearance of magnetism usually occurs in a range of pressure (e.g. Chen et al., 2018, 2014). For Fe_3P , we marked 21.5–24.8 GPa, where the majority of magnetism disappeared, as the pressure of magnetic transition; but it may start far earlier than the marked pressure range. Comparing the SMS at 11.4 GPa with the SMS at 16.5 GPa, we find that some de-

tailed features in the SMS spectra are quite different. There is an emerging peak at about 45 ns and 100 ns at 16.5 GPa. The peak intensities of the three peaks between 50–80 ns also decreases continuously before the sudden collapse at 24.8 GPa. These features indicate that the magnetic transition is a continuous process likely due to the different transition pressures of the three Fe sites. The pressure range is close to that of the magnetic transition at 18.3 GPa–40 GPa reported in previous XRD and XES studies (Gu et al., 2014; 2016). The normalized lattice parameters as a function of pressure were plotted in Fig. 4a. The linear compressibilities of a and c axis are quite similar at low pressures and the c axis becomes less compressible than the a axis at higher pressures, which can be explained by the magnetic transitions (Gu et al., 2014). The magnetic transition is reflected in the changes of the c/a axial ratio with pressure (Fig. 4b). The slope of c/a ratio starts to vary at about 12 GPa, which might be the initiation of the magnetic transition in one Fe site. The c/a ratio increased dramatically between 21.4 GPa and 30.5 GPa, which might be due to the subsequent magnetic transitions of the other two Fe sites at higher pressures

Table 1Elastic properties of Fe₃P and other Fe alloys with similar structures.

Phase	<i>P</i> range (GPa)	<i>K</i> ₀ (GPa)	<i>K</i> ' ₀	<i>V</i> ₀ (Å ³)	Methods	Reference
Fe ₃ P ^a	0–21.4	162.1(5)	4 (fixed)	370.42(4)	SCXRD	This study
Fe ₃ P ^a	0–21.4	162.4(7)	4 (fixed)	370.38(6)	SCXRD+PXRD	This study
Fe ₃ P ^b	30.5–40.7	181(9)	4 (fixed)	364(2)	SCXRD	This study
Fe ₃ P ^b	30.5–111	220(6)	4 (fixed)	357(1)	SCXRD+PXRD	This study
Fe ₃ P	0–20	159(10)	4.4	367.2(3)	PXRD	Gu et al., 2014
Fe ₃ P	0–8	159(1)	4 (fixed)	–	PXRD	Scott et al., 2007
Fe _{2.15} Ni _{0.85} P	0–50	185(1)	4 (fixed)	365.8 (1)	SCXRD	He et al., 2018
Fe ₃ S ^c	0–197	155.6(8)	4 (fixed)	377.0(2) (fixed) ^d	PXRD	Kamada et al., 2014
Fe ₃ S ^c	0–197	125.3(17)	5.1(1)	377.0(2) (fixed) ^d	PXRD	Kamada et al., 2014

^a Magnetic phase of Fe₃P.^b Non-magnetic phase of Fe₃P.^c Fitting to the combined data set from (Chen et al., 2007; Kamada et al., 2014; Seagle et al., 2006).^d *V*₀ is fixed to the value reported by Fei et al. (2000).

(Fig. 4b). The slope of the *c/a* ratio as a function pressure then became flattened after the transition (Fig. 4b). Similar changes in the *c/a* ratio between 20–27 GPa, likely due to the magnetic transition, were also reported for Fe₃S, which is isostructural to Fe₃P (Chen et al., 2007; Kamada et al., 2014), but there is no obvious volume anomaly across the pressure interval for the magnetic transition in Fe₃S (Chen et al., 2007; Kamada et al., 2014). From previous XES studies of Fe₃P and Fe₃S (Gu et al., 2016; Shen et al., 2003), the magnetic transition is highly possible pertinent to the spin transition of Fe. Spin transition is a first-order transition which will cause volume discontinuity. It may occur in a range of pressure (e.g. Chen et al., 2018, 2014). The deviatoric stress onto the sample may widen the transition pressure range, which makes the volume discontinuity difficult to be resolved (e.g. Weis et al., 2017). Small volume anomaly may be not resolvable in the previous study of Fe₃S from XRD measurements (Chen et al., 2007). In the present study, we employed the single-crystal XRD and compressed the single crystal sample more hydrostatically with a small pressure interval, providing a more appropriate way for determining the subtle volume collapse across the magnetic transition.

The *P*–*V* data of the magnetic phase up to 21.4 GPa and at 300 K (Tables S3 & S4) were fitted by the 2nd-order B–M EoS weighted by both the uncertainties in pressure and volume, yielding a bulk modulus *K*_{T0} = 162.4(7) GPa, its first derivative *K*'_{T0} = 4.0 (fixed) and zero pressure volume *V*₀ = 370.38(6) Å³ (Table 1; Figs. 2 & S3). Single-crystal data (run-1) were also fitted by the 2nd-order B–M EoS alone. EoS parameters obtained by fitting both the powder and single-crystal data are consistent with those obtained by fitting only the single-crystal data within uncertainties (Table 1).

The *P*–*V* data of the non-magnetic phase from 30.5 to 111 GPa (Tables S3, S4 and S5) were fitted by the 2nd-order B–M EoS: *K*_{T0} = 220(6) GPa, *K*'_{T0} = 4 (fixed), and *V*₀ = 357(1) Å³. The single-crystal data from 30.5 to 40 GPa were also fitted alone by the 2nd-order B–M EoS (Table 1; Figs. 2 & S3), however, the obtained *K*_{T0} is not well constrained due to the limited pressure range (~10 GPa). We therefore used the *K*_{T0} and *V*₀ obtained from the fitting of all data for comparison as well as for sound velocity calculations combined with our NRIXS results. *K*_{T0} of the non-magnetic phase of Fe₃P is larger than that of the magnetic phase; that is, it became stiffened after the magnetic transition. It indicates that the magnetic transition has a non-negligible effect on the compressibility of Fe₃P, especially when extrapolating to inner core pressures. Therefore, the extrapolation of density to the core pressures needs to be performed using EoS of the non-magnetic phase. Assuming P to be the sole light element in the inner core and the inner core to be composed of a mixture of Fe + Fe₃P, we calculated the P amount in the inner core (Fig. 5). We first calculated the densities of Fe and Fe₃P at 300 K at core

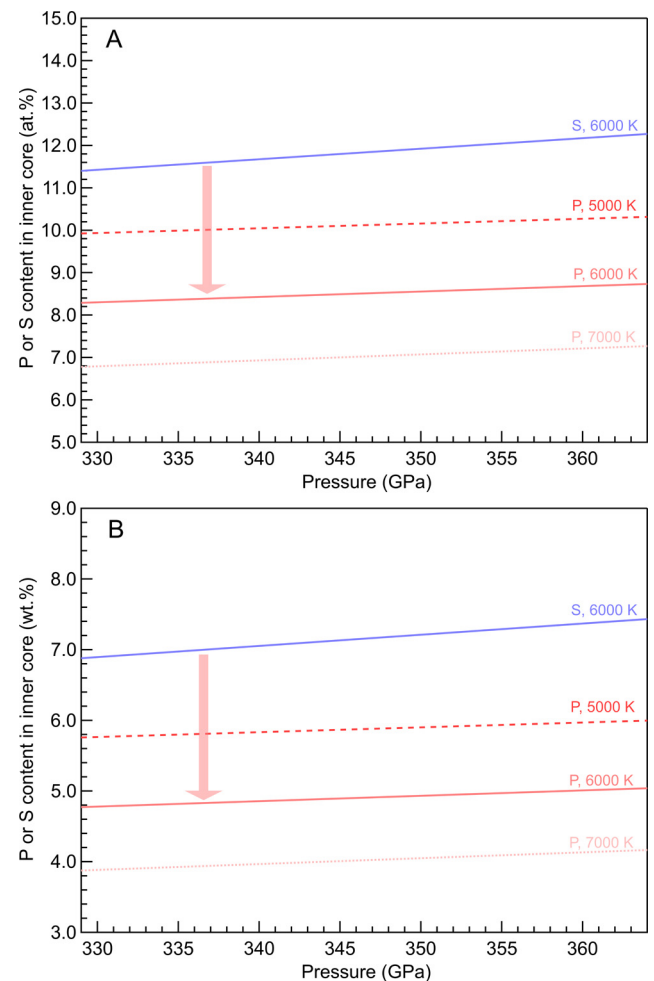


Fig. 5. The estimated P content in Earth's inner core, assuming P is the only element in Earth's inner core. The estimated S content at 6000 K based on the similar assumption was plotted for comparison (Kamada et al., 2014). (A) The estimated content in atomic percent. (B) The estimated content in weight percent.

pressures based on the equation of state of hcp Fe at 300 K (Mao et al., 1990) and equation of state of non-magnetic Fe₃P in this study. The densities of Fe at 5000 K, 6000 K and 7000 K at high pressures were then calculated by the Mie-Grüneisen-Debye equation of state (Seagle et al., 2006). Since the thermal expansivity of Fe₃P was not available at high pressures, we estimate the density of Fe₃P at high temperatures by considering $\Delta P_{\text{thermal}} = \alpha K_T \Delta T$, using $\alpha K_T = 0.011$ for Fe₃S (Seagle et al., 2006). By assuming that α of Fe₃P is the same with that of Fe₃S, αK_T was calculated to be

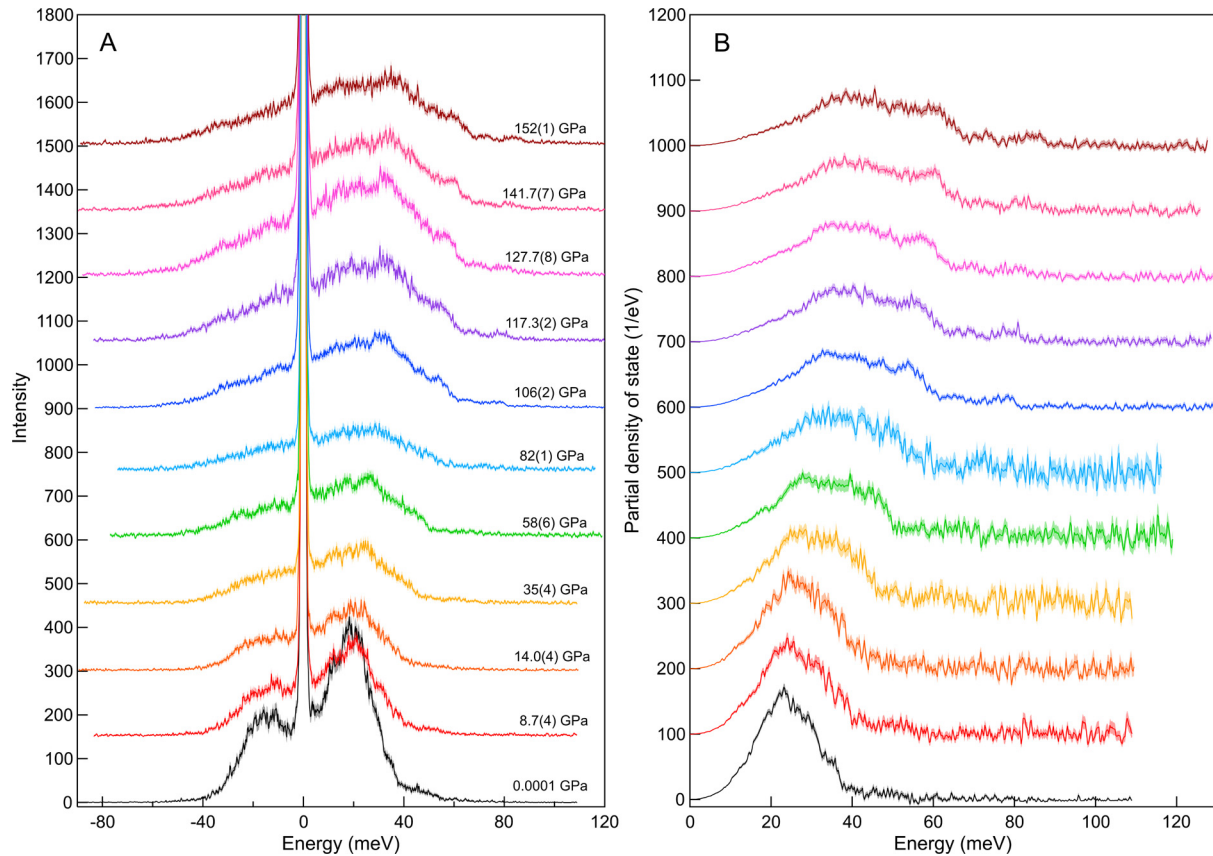


Fig. 6. (A) NRIXS spectra of Fe in Fe₃P up to 152 GPa and at 300K. (B) Derived partial density of state (PDOS) of Fe in Fe₃P. Uncertainties are presented by shaded bands. Vertical offset is applied to the spectra at high pressures for clarity.

0.016 for Fe₃P (Fig. S4). To account for the density deficit of the inner core, the P content at 7000–5000 K in the inner core was estimated to be 3.9 wt.% (8.5 at.%)–6.0 wt.% (14.5 at.%) (Fig. 5). This estimated content is based on the simple assumption that P is the sole light element in the inner core.

3.2. Seismic properties of Fe₃P up to 1.5 Mbar

NRIXS measurements of ⁵⁷Fe₃P were carried out up to 152 GPa and PDOS was derived from the NRIXS data at each pressure (Fig. 6). For harmonic solids, a parabolic fitting of the low-energy portion of PDOS provides an approximation to the bulk Debye sound velocity (V_D) (Sturhahn and Jackson, 2007). The EoS parameters of Fe₃P obtained by our XRD experiments (Table 1) were utilized as input parameters to the program to calculate density (ρ) at given pressure. Using the V_D from the NRIXS measurements and ρ and K_{T0} from the XRD measurements, we derived the compressional-wave velocity (V_P) and shear-wave velocity (V_S) of isotropic aggregate of Fe₃P using the following relations:

$$\frac{3}{V_D^3} = \frac{1}{V_P^3} + \frac{2}{V_S^3} \quad (1)$$

$$\frac{K_S}{\rho} = V_P^2 - \frac{4}{3}V_S^2 \quad (2)$$

where the adiabatic bulk modulus (K_S) is approximated by K_T (K_T and K_S differ by less than 1% at 300 K) (Chen et al., 2014). Equations (1) and (2) have general solutions (Sturhahn and Jackson, 2007):

$$V_S = 0.952V_D - 0.041\sqrt{\frac{K_S}{\rho}} \quad (3)$$

$$V_P = 0.908\sqrt{\frac{K_S}{\rho}} + 0.297V_D - 0.243V_D^2/\sqrt{\frac{K_S}{\rho}} \quad (4)$$

which are accurate to better than 0.1%. From the general solutions, V_S is relatively insensitive to the EoS parameters and V_D determined by NRIXS weighs heavily on V_S . Thus V_S can be derived more precisely from the NRIXS method than V_P , with the latter weighing heavily on the equation of state. (Mao et al., 2004; Sturhahn and Jackson, 2007).

The sound velocities (V_P and V_S) and shear moduli (G) of Fe₃P were determined up to 152 GPa at 300 K (Fig. 7). Comparing the parameters before and after the magnetic transition, there is an obvious jump in K_T and V_P , and a slight softening of G and V_S in Fe₃P (Fig. 7). V_S decreases after the magnetic transition, when comparing V_S of the magnetic phase with extended V_S of non-magnetic phase to lower pressures (Fig. 7D). The slope of V_S versus ρ increases obviously after the magnetic transition (Fig. 8). Fe₃S also has a magnetic transition at 21 GPa, in which both V_P and V_S drop and the velocity-density slope decreases after the magnetic transition in the previous NRIXS studies (Lin et al., 2004). Compared to Fe₃S, the magnetic transition of Fe₃P appears to have strong but relatively different effect on its elastic properties.

The sound velocities of Fe₃P, Fe₃S, Fe, Fe₃C and Fe₇C₃ as a function of ρ are plotted in Fig. 8, which shows that V_P and ρ of Fe₃P follows the Birch's empirical relationship (Birch, 1964): V_P (km/s) = 1.008(21) × ρ (g/cm³) – 1.27(20) ($R^2 = 0.998$) and that the V_S – ρ relationship is also linear: V_S (km/s) = 0.353(33) × ρ (g/cm³) – 0.05(32) ($R^2 = 0.952$). Extrapolating to the inner core pressures by Birch's relationship, we found that the V_P of Fe₃P are similar to that of Fe₃S, but much lower than that of Fe (Mao et al., 2001; Murphy et al., 2013) (Figs. 7 & 8). However, V_S of Fe₃P are much lower than Fe₃S and Fe (Figs. 7 & 8). Thus far

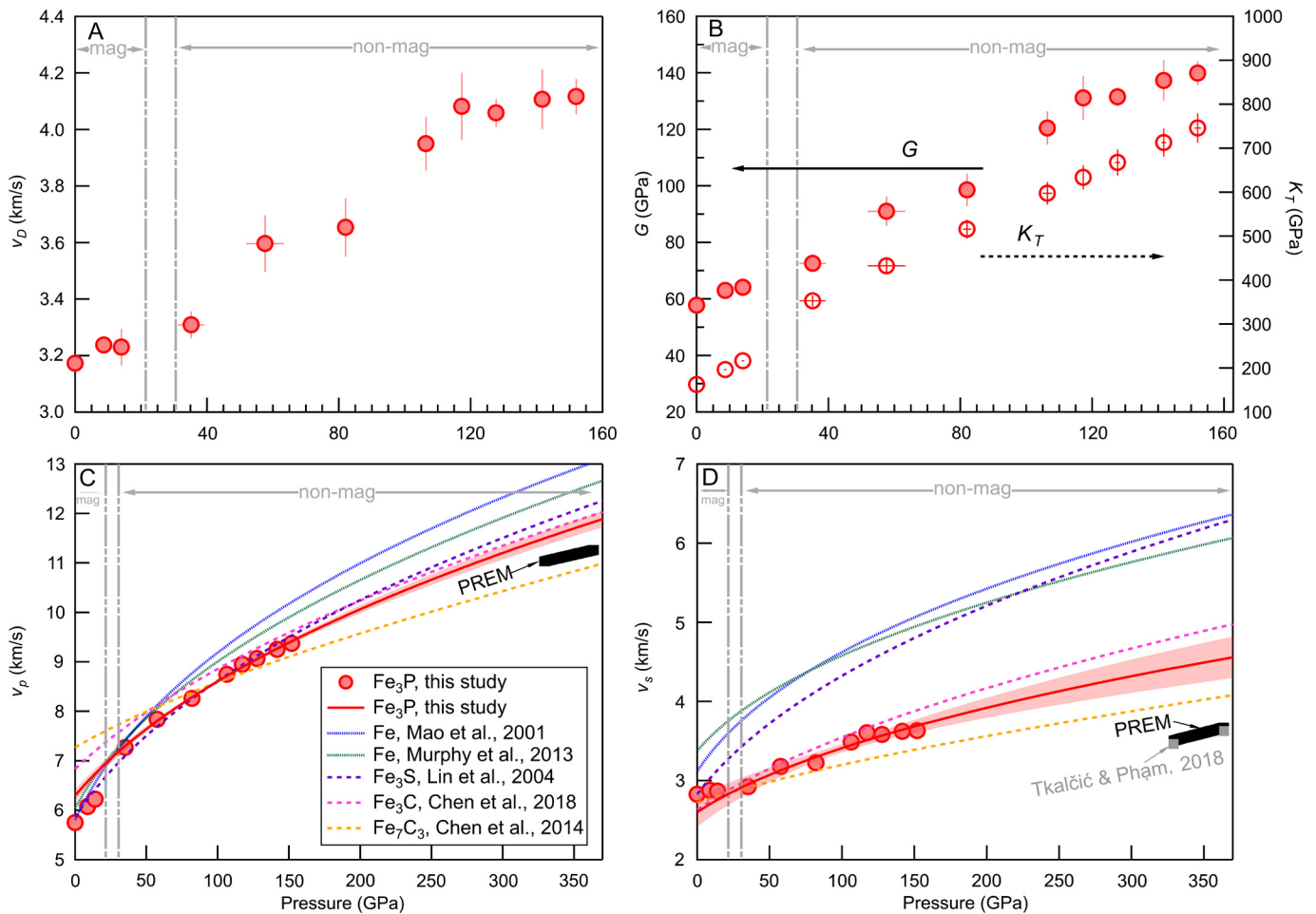


Fig. 7. Sound velocities and elastic moduli determined by NRIXS up to 152 GPa. The relations between V_P or V_S and pressure of Fe_3S , Fe, Fe_3C , Fe_7C_3 , seismic models were also plotted for comparison (Chen et al., 2018, 2014; Dzierwonski and Anderson, 1981; Lin et al., 2004; Mao et al., 2001; Murphy et al., 2013; Tkalcic and Pham, 2018). (A) Debye sound velocity (V_D) of Fe_3P as a function of pressure. (B) Shear modulus (open symbols) and bulk modulus (solid symbols) of Fe_3P as a function of pressure. (C) Compressional velocity (V_P) of Fe_3P , PREM and other iron or iron alloys as a function of pressure. Fitting lines in (C, D) are combining the linear relation between the sound velocity and the density according to Fig. 8 with their equation of states, and shaded areas represent 95% confidence intervals. Vertical dashed lines represent the starting and ending pressures of the magnetic transition. mag: magnetic phase; non-mag: non-magnetic phase.

V_S of Fe_3P is the second lowest among all light element alloys reported after Fe_7C_3 (Chen et al., 2014), indicating that P can reduce V_S effectively. V_S can be derived from $\sqrt{\frac{G}{\rho}}$, while the density can be obtained by the equation of state. The theory of predicting G , especially its pressure dependence is not well understood. The reduction of V_S of Fe_3P may be due to the strong metallic bonds in Fe_3P . The covalent bonds are directional while the metallic bonds are not directional, thus strong metallic bonds may lead to smaller G . Fe_3P is dominated by metallic bonds indicated by the metallic-type response on electrical conductivity (resistance increases with temperature) (Yin et al., 2019b). Theoretical calculation of Fe_3P also indicates that it is dominant in metallic bonds, which leads to lower G and V_S compared with other Fe-P alloy (Wu et al., 2015). From the electron density distribution map of Fe_3P , the covalent bonds still exist in Fe-P alloy locally (Wu et al., 2015). There is no report about the electrical conductivity or bond type of Fe_3S . Considering Fe_3S is isostructural with Fe_3P , they may share the similar types of bonding with Fe_3P . S has higher electronegativity than P which may result in stronger electron localization (stronger covalent bond) in Fe_3S than Fe_3P , likely making the G of Fe_3S higher than Fe_3P . However, density and spin state also play a role in affecting the sound velocities. The data for the isostructural Fe_3S , V_P and V_S , are only collected up to ~ 60 GPa (Lin et al., 2004). With only one set of data for Fe_3P and Fe_3S , more

systematic and comprehensive studies are required before we can provide a mechanism conclusively. Thus, there is no simple answer for the mechanism of reduction of V_S by the addition of certain light element.

4. Geophysical implications

The magnetic transition of Fe_3P significantly affects its elastic properties, that is, ρ , K , and G , as well as V_P and V_S . Physical properties of Fe_3P after the magnetic transition needs to be utilized for the discussion of Earth's core. At inner core pressures and 300 K, the extrapolated densities of the non-magnetic Fe_3P are lower than those of Fe and iron alloys such as Fe_3S (Fig. 8). Therefore, the presence of Fe_3P in the inner core may partly account for the inner core "density deficit" (Fig. 8). Geochemical arguments indicate that the Earth's core is estimated to contain 0.2–0.5 wt.% P, whereas the estimate on the concentration of S is 1.9 wt.% (McDonough, 2003; McDonough and Sun, 1995). To account for the density deficit by Fe_3S at core pressures, the S content was estimated to be 5.1 wt.%–6.9 wt.% at 7000 K and 6000 K at inner core boundary pressure, respectively, assuming that S is the sole light element in the inner core in the form of Fe_3S coexisting with Fe (Kamada et al., 2014). In this study, density at core pressures can be calculated by the EoS of the non-magnetic phase of Fe_3P . To

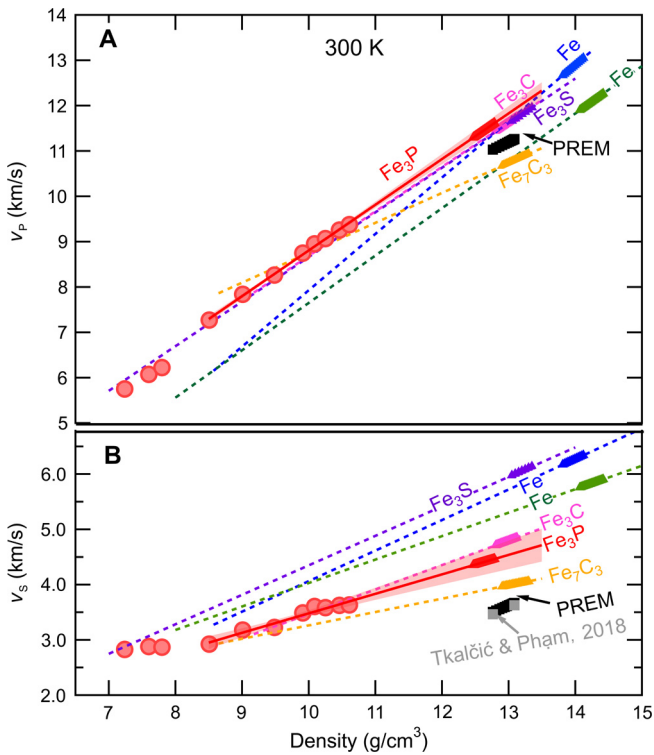


Fig. 8. Sound velocities of Fe₃P, Fe₃S, Fe, Fe₃C, Fe₇C₃ and seismic models as a function of density. (A) Compressional velocity (V_P) and (B) Shear velocity (V_S) of Fe₃P (this study), Fe₃S (Lin et al., 2004), hcp Fe (Mao et al., 2001), hcp Fe (Murphy et al., 2013), Fe₃C (Chen et al., 2018), Fe₇C₃ (Chen et al., 2014), PREM model (Dziewonski and Anderson, 1981) and a seismic study by Tkalčić and Pham (2018). Solid and dashed lines are linear fitting lines, and shaded area represent 95% confidence intervals. The solid bars represent the densities of iron alloys at inner core pressures and 300 K (Chen et al., 2007, 2012; Dewaele et al., 2006; Kamada et al., 2014; Mao et al., 1990).

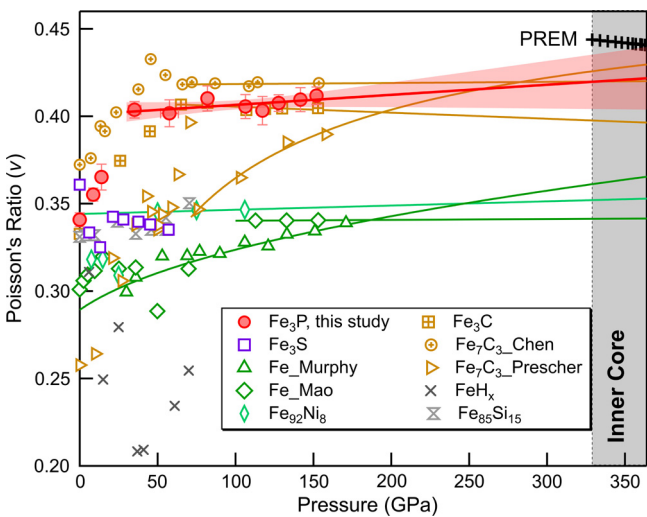


Fig. 9. Pressure dependence of Poisson's ratio of Fe₃P (this study), Fe₃S (Lin et al., 2004), Fe (Mao et al., 2001; Murphy et al., 2013), Fe₉₂Ni₈ (Lin et al., 2003), Fe₃C (Chen et al., 2018), Fe₇C₃ (Chen et al., 2014), FeH_x (Shibazaki et al., 2012) and Fe₈₅Si₁₅ (Lin et al., 2003) at 300 K. Solid lines are fitting lines, and the shaded area represents the 95% confidence interval. The Poisson's ratio of PREM is also plotted for comparison.

match the density of the Earth's inner core in the PREM model assuming that P is the sole light element in the inner core, 3.9 wt.% (8.5 at.%)–6.0 wt.% (14.5 at.%) P was required. Take the densities at 6000 K for example, 30%–32% by weight (27%–29% by mole) less P than S was needed to account for the density deficit. Fe₃P and Fe₃S

were found to form the solid solutions at high pressures (Stewart and Schmidt, 2007; Gu et al., 2016). Therefore instead of considering P and S individually, a Fe₃(S,P) solid solution may be a more realistic component for the inner core, and the addition of Fe₃P into Fe₃S can help account for the core density deficit.

V_S of the inner core from the PREM model are lower than those of Fe at core pressures (Mao et al., 2001). A recent work (Tkalčić and Pham, 2018) concludes that there is a “squishy” solid inner core with an even smaller shear modulus and 2.5% lower shear velocity compared with PREM, which further enlarges the discrepancy (Figs. 7 & 8). The presence of melt (Singh et al., 2000), pre-melting effect (Martorell et al., 2013), anelasticity (Vočadlo, 2007), texture effect (Antonangeli et al., 2004), and the presence of light elements such as carbon and silicon (Chen et al., 2014; Li et al., 2018) have been proposed to explain the anomalously low V_S of the inner core. We found that V_S of non-magnetic Fe₃P are among the lowest at inner core pressures in addition to Fe₃C and Fe₇C₃ (Chen et al., 2018, 2014; Prescher et al., 2015) (Fig. 8), in comparison with other iron alloys (Lin et al., 2004, 2003; Shibazaki et al., 2012). If this relationship is similar at high temperatures, Fe₃P may partly account for the shear wave velocity discrepancy of the core with respect to Fe. The addition of P into Fe₃S may also effectively lower its V_S . Fe₃(S,P), therefore, may serve as a candidate of the Earth's solid inner core.

The Poisson's ratio (ν) can be calculated using the V_P and V_S ratio or K and G by equation (5):

$$\nu = \frac{(V_P/V_S)^2 - 2}{2[(V_P/V_S)^2 - 1]} = \frac{1}{2} - \frac{3}{6\frac{K}{G} + 2} \quad (5)$$

ν of Fe₃P and Fe₃S are close to each other at ambient conditions while they seemingly deviate at higher pressures based on the current data coverage (Fig. 9). The slope of ν versus ρ of Fe₃P is steep before the magnetic transition and becomes flattened after the magnetic transition. Based on the limited data of Fe₃S, it appears that ν of Fe₃S drops rapidly with density and the ν - ρ slope becomes flattened after the magnetic transition. The high Poisson's ratio (ν) of Fe₃P is due to the large K and small G for the non-magnetic phase of Fe₃P (Table 1 and Fig. 9). The extrapolated ν of Fe₃P of 0.42 at inner core pressures, which is remarkably higher than those of Fe and Fe₃S and close to that by PREM ($\nu = 0.45$) (Fig. 9), although the temperature effect still needs further investigations.

The composition of the core is the key to understand the cycling and distribution of volatiles in the deep Earth during the formation of Earth's core. The light constituents in the core are considered to play an important role in sustaining the geodynamo, responsible for the generation of the Earth's magnetic field and thus allowing our Earth to evolve into a habitable planet. Elastic and magnetic properties of inner core candidate Fe₃P up to 1.5 Mbar were investigated in the DACs combined with multiple synchrotron-based techniques—powder and single-crystal XRD, SMS, and NRXIS. Our results suggested that Fe₃P bears low density, anomalously low V_S and high Poisson's ratio at core pressures. As a result, Fe₃P may lower the V_S and density of Fe₃S when forming a solid solution Fe₃(S,P) at core pressures, which can better match the sound velocity and density profile of the inner core within the geochemical constraints. It implies that the primordial P may have largely entered the Earth's core, which also explains the deficit of P in the Earth's crust and mantle. According to the phase diagrams of Fe–P system at 23 GPa (Stewart and Schmidt, 2007), P would be concentrated in liquid Fe if the P content of the core is lower than the eutectic composition (~9 wt.%). Conversely, if the P content is higher than the eutectic composition, P would be concentrated in the solid phase as Fe₃P during the solidification of the Fe–P liquid. By comparing the phase diagrams at 3 and 23 GPa, the P content in the eutectic composition appears to decrease with pressure

(Stewart and Schmidt, 2007; Yin et al., 2019a). If this trend persists to core pressures, it is possible that at core pressure, the P content may fall in the right side of eutectic point. In addition, the introduction of S to the Fe–P system to form Fe–S–P solid solutions, i.e., Fe₃(S,P), may affect the phase diagram significantly, likely facilitating the incorporation of P in the solid inner core. Further investigations on the Fe–S–P phase diagram and the elastic properties of Fe₃P, Fe–S–P alloys such as Fe₃(S,P) at simultaneous high-pressure and high-temperature conditions should be carried out to constrain the composition of our Earth's or planetary cores.

Declaration of competing interest

The authors declare that they have no known competing financial interests or personal relationships that could have appeared to influence the work reported in this paper.

Acknowledgements

We thank two anonymous reviewers for their constructive comments which improved the manuscript. B. Chen acknowledges the support from the U.S. National Science Foundation (NSF) (EAR-1555388 and EAR-1829273). This research used resources of the Advanced Photon Source (APS), a U.S. Department of Energy (DOE) Office of Science User Facility operated for the DOE Office of Science by Argonne National Laboratory under Contract No. DE-AC02-06CH11357. GeoSoilEnviroCARS (Sector 13) is supported by NSF-Earth Sciences (EAR-1128799), and the Department of Energy, Geosciences (DE-FG02-94ER14466). The use of gas loading system was supported by GeoSoilEnviroCARS and by the Consortium for Materials Properties Research in Earth Sciences (COMPRES) under NSF Cooperative Agreement EAR-1606856. Sector 3 (APS) operations are supported in part by COMPRES under NSF Cooperative Agreement EAR-1606856. Use of the COMPRES Cell Assembly Project was supported by COMPRES under NSF Cooperative Agreement EAR-1661511.

Appendix A. Supplementary material

Supplementary material related to this article can be found online at <https://doi.org/10.1016/j.epsl.2019.115974>.

References

- Akahama, Y., Kawamura, H., 2006. Pressure calibration of diamond anvil Raman gauge to 310 GPa. *J. Appl. Phys.* 100, 043516.
- Antonangeli, D., Occelli, F., Requardt, H., Badro, J., Fiquet, G., Krisch, M., 2004. Elastic anisotropy in textured hcp-iron to 112 GPa from sound wave propagation measurements. *Earth Planet. Sci. Lett.* 225, 243–251.
- Birch, F., 1964. Density and composition of mantle and core. *J. Geophys. Res.* 69, 4377–4388.
- Chen, B., Gao, L., Funakoshi, K.-i., Li, J., 2007. Thermal expansion of iron-rich alloys and implications for the Earth's core. *Proc. Natl. Acad. Sci.* 104, 9162–9167.
- Chen, B., Gao, L., Lavina, B., Dera, P., Alp, E.E., Zhao, J., Li, J., 2012. Magneto-elastic coupling in compressed Fe₇C₃ supports carbon in Earth's inner core. *Geophys. Res. Lett.* 39.
- Chen, B., Li, Z., Zhang, D., Liu, J., Hu, M.Y., Zhao, J., Bi, W., Alp, E.E., Xiao, Y., Chow, P., 2014. Hidden carbon in Earth's inner core revealed by shear softening in dense Fe₇C₃. *Proc. Natl. Acad. Sci.* 111, 17755–17758.
- Chen, B., Lai, X., Li, J., Liu, J., Zhao, J., Bi, W., Alp, E.E., Hu, M.Y., Xiao, Y., 2018. Experimental constraints on the sound velocities of cementite Fe₃C to core pressures. *Earth Planet. Sci. Lett.* 494, 164–171.
- Dera, P., Zhuravlev, K., Prakapenka, V., Rivers, M.L., Finkelstein, G.J., Grubor-Urosevic, O., Tschauner, O., Clark, S.M., Downs, R.T., 2013. High pressure single-crystal micro X-ray diffraction analysis with GSE_ADA/RSV software. *High Press. Res.* 33, 466–484.
- Dewaele, A., Loubeyre, P., Occelli, F., Mezouar, M., Dorogokupets, P.I., Torrent, M., 2006. Quasihydrostatic equation of state of iron above 2 Mbar. *Phys. Rev. Lett.* 97, 215504.
- Dziewonski, A.M., Anderson, D.L., 1981. Preliminary reference Earth model. *Phys. Earth Planet. Inter.* 25, 297–356.
- Fei, Y., Li, J., Bertka, C.M., Prewitt, C.T., 2000. Structure type and bulk modulus of Fe₃S, a new iron-sulfur compound. *Am. Mineral.* 85, 1830–1833.
- Filippelli, G.M., 2008. The global phosphorus cycle: past, present, and future. *Elements* 4, 89–95.
- Gu, T., Fei, Y., Wu, X., Qin, S., 2014. High-pressure behavior of Fe₃P and the role of phosphorus in planetary cores. *Earth Planet. Sci. Lett.* 390, 296–303.
- Gu, T., Fei, Y., Wu, X., Qin, S., 2016. Phase stabilities and spin transitions of Fe₃(S_{1-x}P_x) at high pressure and its implications in meteorites. *Am. Mineral.* 101, 205–210.
- He, X.-J., Guo, J.-Z., Wu, X., Huang, S.-X., Qin, F., Gu, X.-P., Qin, S., 2018. Compressibility of natural schreibersite up to 50 GPa. *Phys. Chem. Miner.*, 1–9.
- Kamada, S., Ohtani, E., Terasaki, H., Sakai, T., Takahashi, S., Hirao, N., Ohishi, Y., 2014. Equation of state of Fe₃S at room temperature up to 2 megabars. *Phys. Earth Planet. Inter.* 228, 106–113.
- Li, J., Fei, Y., 2014. Experimental constraints on core composition. In: Holland, H.D., Turekian, K.K. (Eds.), *Treatise on Geochemistry*, second edition. Elsevier, Oxford, pp. 527–557.
- Li, Y., Vočadlo, L., Brodholt, J.P., 2018. The elastic properties of hcp-Fe alloys under the conditions of the Earth's inner core. *Earth Planet. Sci. Lett.* 493, 118–127.
- Lin, J.-F., Fei, Y., Sturhahn, W., Zhao, J., Mao, H.-k., Hemley, R.J., 2004. Magnetic transition and sound velocities of Fe₃S at high pressure: implications for Earth and planetary cores. *Earth Planet. Sci. Lett.* 226, 33–40.
- Lin, J.F., Struzhkin, V.V., Sturhahn, W., Huang, E., Zhao, J., Hu, M.Y., Alp, E.E., Mao, N.k., Bostor, H., Hemley, R.J., 2003. Sound velocities of iron-nickel and iron-silicon alloys at high pressures. *Geophys. Res. Lett.* 30, 2112.
- Mao, H., Xu, J.-A., Bell, P., 1986. Calibration of the ruby pressure gauge to 800 kbar under quasi-hydrostatic conditions. *J. Geophys. Res., Solid Earth* 91, 4673–4676.
- Mao, H., Wu, Y., Chen, L., Shu, J., Jephcoat, A.P., 1990. Static compression of iron to 300 GPa and Fe_{0.8}Ni_{0.2} alloy to 260 GPa: implications for composition of the core. *J. Geophys. Res., Solid Earth* 95, 21737–21742.
- Mao, H., Xu, J., Struzhkin, V., Shu, J., Hemley, R., Sturhahn, W., Hu, M., Alp, E., Vočadlo, L., Alfè, D., 2001. Phonon density of states of iron up to 153 gigapascals. *Science* 292, 914–916.
- Mao, W.L., Sturhahn, W., Heinz, D.L., Mao, H.K., Shu, J., Hemley, R.J., 2004. Nuclear resonant x-ray scattering of iron hydride at high pressure. *Geophys. Res. Lett.* 31, L15618.
- Martorell, B., Vočadlo, L., Brodholt, J., Wood, I.G., 2013. Strong premelting effect in the elastic properties of hcp-Fe under inner-core conditions. *Science* 342, 466–468.
- McDonough, W., 2003. Compositional model for the Earth's core. In: Holland, H.D., Turekian, K.K. (Eds.), *Treatise Geochemistry*. Elsevier, Oxford, pp. 547–568.
- McDonough, W.F., Sun, S.-S., 1995. The composition of the Earth. *Chem. Geol.* 120, 223–253.
- Murphy, C.A., Jackson, J.M., Sturhahn, W., 2013. Experimental constraints on the thermodynamics and sound velocities of hcp-Fe to core pressures. *J. Geophys. Res., Solid Earth* 118, 1999–2016.
- Osadchii, E.G., Novikov, G., Baryshnikova, G., 1981. The Elga meteorite-silicate inclusions and shock metamorphism. *Proc. Lunar Planet. Sci. Conf.*, 1049–1068.
- Prescher, C., Prakapenka, V.B., 2015. DIOPTAS: a program for reduction of two-dimensional X-ray diffraction data and data exploration. *High Press. Res.* 35, 223–230.
- Prescher, C., Dubrovinsky, L., Bykova, E., Kuznetsov, I., Glazyrin, K., Kantor, A., McCammon, C., Mookherjee, M., Nakajima, Y., Miyajima, N., 2015. High Poisson's ratio of Earth's inner core explained by carbon alloying. *Nat. Geosci.* 8, 220–223.
- Scott, H.P., Huggins, S., Frank, M.R., Maglio, S.J., Martin, C.D., Meng, Y., Santillán, J., Williams, Q., 2007. Equation of state and high-pressure stability of Fe₃P-schreibersite: implications for phosphorus storage in planetary cores. *Geophys. Res. Lett.* 34, L06302.
- Seagle, C.T., Campbell, A.J., Heinz, D.L., Shen, G., Prakapenka, V.B., 2006. Thermal equation of state of Fe₃S and implications for sulfur in Earth's core. *J. Geophys. Res., Solid Earth* 111, B06209.
- Seto, Y., 2010. Development of a software suite on X-ray diffraction experiments. *Rev. High Press. Sci. Technol.* 20, 269–276.
- Sheldrick, G.M., 2008. A short history of SHELX. *Acta Crystallogr. A, Found. Crystallogr.* 64, 112–122.
- Shen, G., Lin, J., Fei, Y., Mao, H., Hu, M., Chow, P., 2003. Magnetic and structural transition in Fe₃S at high pressures. *Eos Trans. AGU* 84 (46), F1548–F1549 (Fall Meet. Suppl., Abstract V31E-0961).
- Shibazaki, Y., Ohtani, E., Fukui, H., Sakai, T., Kamada, S., Ishikawa, D., Tsutsui, S., Baron, A.Q., Nishitani, N., Hirao, N., 2012. Sound velocity measurements in dhcp-FeH up to 70 GPa with inelastic X-ray scattering: implications for the composition of the Earth's core. *Earth Planet. Sci. Lett.* 313, 79–85.
- Singh, S., Taylor, M., Montagner, J., 2000. On the presence of liquid in Earth's inner core. *Science* 287, 2471–2474.
- Stewart, A., Schmidt, M., 2007. Sulfur and phosphorus in the Earth's core: the Fe–P–S system at 23 GPa. *Geophys. Res. Lett.* 34, L13201.
- Sturhahn, W., 2000. CONUSS and PHOENIX: evaluation of nuclear resonant scattering data. *Hyperfine Interact.* 125, 149–172.
- Sturhahn, W., 2004. Nuclear resonant spectroscopy. *J. Phys. Condens. Matter* 16, S497.

- Sturhahn, W., Jackson, J.M., 2007. Geophysical applications of nuclear resonant spectroscopy. In: Special Paper 421: Advances in High-Pressure Mineralogy. Geological Society of America, pp. 157–174.
- Tkalčić, H., Phạm, T.-S., 2018. Shear properties of Earth's inner core constrained by a detection of J waves in global correlation wavefield. *Science* 362, 329–332.
- Toby, B.H., Von Dreele, R.B., 2013. GSAS-II: the genesis of a modern open-source all purpose crystallography software package. *J. Appl. Crystallogr.* 46, 544–549.
- Vočadlo, L., 2007. Ab initio calculations of the elasticity of iron and iron alloys at inner core conditions: evidence for a partially molten inner core? *Earth Planet. Sci. Lett.* 254, 227–232.
- Wasson, J.T., 2012. *Meteorites: Classification and Properties*. Springer Science & Business Media.
- Weis, C., Sternemann, C., Cerantola, V., Sahle, C.J., Spiekermann, G., Harder, M., Forov, Y., Kononov, A., Sakrowski, R., Yavaş, H., 2017. Pressure driven spin transition in siderite and magnesiosiderite single crystals. *Sci. Rep.* 7, 16526.
- Wu, J., Chong, X., Zhou, R., Jiang, Y., Feng, J., 2015. Structure, stability, mechanical and electronic properties of Fe–P binary compounds by first-principles calculations. *RSC Adv.* 5, 81943–81956.
- Yin, Y., Li, Z., Zhai, S., 2019a. The phase diagram of the Fe–P binary system at 3 GPa and implications for phosphorus in the lunar core. *Geochim. Cosmochim. Acta* 254, 54–66.
- Yin, Y., Zhai, K., Zhang, B., Zhai, S., 2019b. Electrical resistivity of iron phosphides at high-pressure and high-temperature conditions with implications for lunar core's thermal conductivity. *J. Geophys. Res., Solid Earth* 124, 5544–5556.